Author Manuscript

Author Manuscript

Author Manuscript

Author Manuscript

HHS Public Access

Author manuscript

J Phys Chem B. Author manuscript; available in PMC 2019 August 20.

Published in final edited form as:

J Phys Chem B. 2016 April 21; 120(15): 3666–3676. doi:10.1021/acs.jpcb.5b12594.

Self-Assembly and Critical Aggregation Concentration Measurements of ABA Triblock Copolymers with Varying B Block Types: Model Development, Prediction and Validation

Fikret Aydin[1,*], **Xiaolei Chu**[1,*], **Geetartha Uppaladadium**[1,*], **David Devore**[2], **Ritu Goyal**[2], **N. Sanjeeva Murthy**[2], **Zheng Zhang**[2], **Joachim Kohn**[2], **Meenakshi Dutt**[1,**]

[1]Department of Chemical Engineering, The State University of New Jersey, Piscataway, New Jersey

[2]New Jersey Center for Biomaterials, Rutgers, The State University of New Jersey, Piscataway, New Jersey

Abstract

The Dissipative Particle Dynamics (DPD) simulation technique is a coarse-grained (CG) Molecular Dynamics-based approach that can effectively capture the hydrodynamics of complex systems while retaining essential information about the structural properties of the molecular species. An advantageous feature of DPD is that it utilizes soft repulsive interactions between the beads, which are CG representation of groups of atoms or molecules. In this study, we used the DPD simulation technique to study the aggregation characteristics of ABA triblock copolymers in aqueous medium. Pluronic® polymers (PEG-PPO-PEG) were modeled as two segments of hydrophilic beads and one segment of hydrophobic beads. Tyrosine-derived PEG_{5K}-b-oligo(desaminotyrosyl tyrosine octyl ester-suberate)-b-PEG_{5K} (PEG_{5k}-oligo(DTO-SA)-PEG_{5k}) block copolymers possess alternate rigid and flexible components along the hydrophobic oligo(DTO-SA) chain, and were modeled as two segments of hydrophilic beads and one segment of hydrophobic, alternate soft and hard beads. The formation, structure, and morphology of the initial aggregation of the polymer molecules in aqueous medium were investigated by following the aggregation dynamics. The dimensions of the aggregates predicted by the computational approach were in good agreement with corresponding results from experiments, for the Pluronic® and PEG_{5k}-oligo(DTO-SA)-PEG_{5k} block copolymers. In addition, DPD simulations were utilized to determine the critical aggregation concentration (CAC), which was compared with corresponding results from an experimental approach. For Pluronic® polymers F68, F88, F108, and F127, the computational results agreed well with experimental measurements of the CAC measurements. For PEG_{5k}-b-oligo(DTO-SA)-b-PEG_{5K} block polymers, the complexity in polymer structure made it difficult to directly determine their CAC values via the CG scheme. Therefore, we determined CAC values of a series of triblock copolymers with 3 to 8 DTO-SA

**Corresponding author: meenakshi.dutt@rutgers.edu.
*Equal contributions

Supporting Information Available

A movie showing the aggregation process of tyrosine-based PEG_{5k}-b-oligo(DTO-SA)-b-PEG_{5k} polymers, a movie showing the dynamic configuration of a single tyrosine-based polymer chain, a movie showing the aggregation process of Pluronic® F127 polymers. This information is available free of charge via the Internet at http://pubs.acs.org.

Author Manuscript Author Manuscript Author Manuscript Author Manuscript

units using DPD simulations, and used these results to predict the CAC values of triblock copolymers with higher molecular weights by extrapolation. In parallel, a PEG_{5K}-b-oligo(DTO-SA)-b-PEG_{5K} block copolymer was synthesized and the CAC value was determined experimentally using the pyrene method. The experimental CAC value agreed well with the CAC value predicted by simulation. These results validate our CG models, and demonstrate an avenue to simulate and predict aggregation characteristics of ABA amphiphilic triblock copolymers with complex structures.

Graphical Abstract

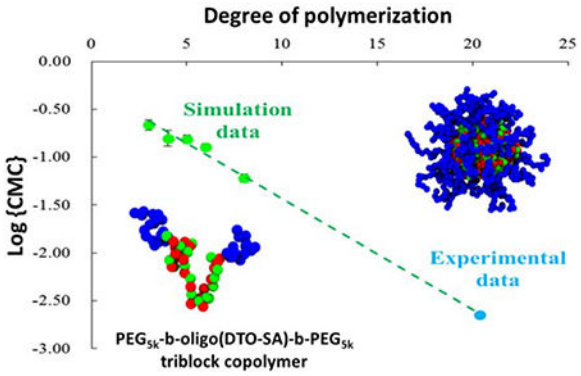

Keywords

Triblock Copolymers; Self-assembly; Critical Aggregation Concentration; Dissipative Particle Dynamics

INTRODUCTION

Nanotechnology enables the manipulation of matter on atomic, molecular, and supramolecular scales involving the design, characterization and application of materials, facilitating novel technological advances in the field of medicine (so called Nanomedicine).[1] Over the last few decades, different types of nanoparticles have been developed based on various components, including carbon, silica oxides, metal oxides, nanocrystals, lipids, polymers, dendrimers, and quantum dots, together with an increasing variety of newly developed materials.[2] Amphiphilic block copolymers form nanoparticles with a core – shell architecture in an aqueous medium.[3] These nanoparticles are promising drug delivery carriers, as the hydrophobic core serves as the reservoir for the incorporation of lipophilic drugs,[4] and the hydrophilic shell (PEG) enables stable dispersion in an aqueous environment. The drug loading efficiency of the nanoparticles is governed by a number of critical parameters, particularly the chemical affinity of the loaded drug for the nanoparticle core.[5] Amphiphilic copolymers can be designed to self-assemble with low critical aggregation concentration (CAC), thus, providing stable aqueous dispersions of lipophilic drugs by maintaining structural integrity and avoiding drug precipitation upon infinite dilution.[6] This is highly important for the practical applications.[7] There are various experimental methods for determination of CAC of polymers.[8]

Author Manuscript Author Manuscript Author Manuscript Author Manuscript

Computational methods encompassing implicit and explicit solvent approaches have been adopted to measure the CAC of block copolymers. A unique advantage of computational methods is the ability to determine CAC values of drug delivery systems based on a virtual library of numerous ABA block polymers. Computational prediction of the CAC requires a model that has been validated and refined to capture the chemistry of the polymer. Stochastic computational techniques such as the Monte Carlo method have been used to determine the CAC of a triblock copolymer using an implicit solvent CG model.[9,10] Deterministic Molecular Dynamics (MD) and MD-based simulation techniques such as Brownian Dynamics and Dissipative Particle Dynamics (DPD) have also been used to calculate the CAC for specific and general diblock and triblock copolymers.[10–11] We use a mesoscopic simulation technique entitled DPD,[12] which bridges molecular properties to the continuum scales, and can capture the hydrodynamic behavior of the system over extended time scales to resolve dynamical processes underlying the formation via self-assembly and the structure of polymeric nanoparticles.

The comparison of CAC values of expansive libraries of ABA block copolymers between experimental and computational approaches is intractable. In this study, two ABA triblock copolymer systems were selected for model development, validation and prediction. One system is Pluronic®, i.e., poly(ethylene glycol)-b-poly(propylene oxide)-b-poly(ethylene glycol) (PEG-PPO-PEG) copolymers,[13] and the other system is tyrosine-based PEG-polyarylate-PEG copolymers, that represents a platform technology of nano-sized carriers for hydrophobic drug delivery.[14] In particular, the polyarylate used in this study is made of oligo(desaminotyrosyltyrosine octyl ester-suberate) [oligo(DTO-SA)]. Coarse-grained models of the block copolymers were developed and used to study the characteristics of the self-assembly and the CAC of these polymeric systems in aqueous environment. In parallel, the CAC of the polymers were also determined experimentally using a well-established fluorescent pyrene probe method.[8c] The coarse-grained models were validated by comparing properties measured by computational and experimental approaches. The tyrosine-based ABA triblock copolymers are entitled tyropsheres.

METHODOLOGY

Materials:

Pluronic® F-68 (Kolliphor® P188), F-108, and F-127 were purchased from Sigma-Aldrich, and Pluronic® F88 was a gift from BASF. Dulbecco's Phosphate Buffered Saline (PBS) and pyrene were purchased from Sigma-Aldrich.

A. Computational Methodology—DPD is a mesoscopic simulation technique that uses soft-sphere coarse-grained models to capture both the molecular details of the nanoscopic building blocks and their supramolecular organization while simultaneously resolving the hydrodynamics of the system over extended time scales.[12,15] In order to capture the dynamics of the soft spheres, the DPD technique integrates Newton's equation of motion via the use of similar numerical integrators as those applied in other deterministic particle-based simulation methods.[12,16] The force acting on a soft sphere i due to its interactions with a neighboring soft sphere j ($j \neq i$) has three components: a conservative

Author Manuscript Author Manuscript Author Manuscript Author Manuscript

force, a dissipative force, and a random force; they operate within a certain cut-off distance r_c from the reference particle i. These forces are pairwise additive and yield the total force acting on particle i, which is given by $\boldsymbol{F}_i = \sum_{j \neq i} \boldsymbol{F}_{ij}^C + \boldsymbol{F}_{ij}^D + \boldsymbol{F}_{ij}^R$. The soft spheres interact via a soft-repulsive force $\left(\boldsymbol{F}_{ij}^C = a_{ij}\left(1 - \frac{r_{ij}}{r_c}\right)\hat{\boldsymbol{r}}_{ij}, \text{for } r_{ij} < r_c \text{ and } \boldsymbol{F}_{ij}^C = 0, \text{for } r_{ij} > r_c\right)$, a dissipative force $\left(\boldsymbol{F}_{ij}^D = -\gamma\omega^d\left(r_{ij}\right)\left(\boldsymbol{r}_{ij}.\boldsymbol{v}_{ij}\right)\hat{\boldsymbol{r}}_{ij}\right)$ and a random force $\left(\boldsymbol{F}_{ij}^R = -\sigma\omega^r\left(r_{ij}\right)\theta_{ij}\hat{\boldsymbol{r}}_{ij}\right)$, where $\omega^d(r) = [w^r(r)]^2 = (1 - r)^2$ (for $r < 1$), $\omega^d(r) = [w^r(r)]^2 = 0$ (for r^3 1) and $\sigma^2 = 2\gamma k_B T$. a_{ij} is the maximum repulsion between spheres i and j, $\boldsymbol{v}_{ij} = \boldsymbol{v}_i - \boldsymbol{v}_j$ is the relative velocity of the two spheres, $\boldsymbol{r}_{ij} = \boldsymbol{r}_i - \boldsymbol{r}_j$, $r_{ij} = |\boldsymbol{r}_i - \boldsymbol{r}_j|$, $\hat{\boldsymbol{r}}_{ij} = \boldsymbol{r}_{ij}/r_{ij}$, $r = r_{ij}/r_c$, γ is the viscosity related parameter used in the simulations, σ is the noise amplitude, $\theta_{ij}(t)$ is a randomly fluctuating variable from Gaussian statistics, ω^d and ω^r are the separation dependent weight functions which become zero at distances greater than or equal to the cutoff distance r_c. Since the local linear and angular momentum is conserved by all of these three forces, even the small systems exhibit hydrodynamic behavior.[12] The constraints imposed on the random and dissipative forces by certain relations ensure that the statistical mechanics of the system conforms to the canonical ensemble.[12,16] The relation between the pair repulsion parameter a_{ij} and the Flory interaction parameter χ for a bead number density $\rho = 3r_c^{-3}$ is given by $\chi = (0.286 \pm 0.002)(a_{ij} - a_{ii})$.[12] The DPD simulations are run using the open source parallelized MD program entitled LAMMPS.[17]

The ABA triblock copolymer molecules are represented by the bead-spring model, as shown in Fig. 1. Two consecutive beads in a chain are connected via a bond that is described by the harmonic spring potential $E_{bond} = K_{bond}((r - b)/r_c)^2$, where K_{bond} is the bond constant and b is the equilibrium bond length. The constants, K_{bond} and b are assigned values of 64ε and $0.5r_c$, respectively.[15a,18]

The soft repulsive pair potential parameters for the hydrophilic and hydrophobic beads are selected to capture their amphiphilic nature. The interaction parameters between the like components, a_{ij}, are based on the property of water.[12] The repulsion parameter between two beads of the same type is set at $a_{ij} = 25$ (measured in units of k_bT/r_c) which is based upon the compressibility of water at room temperature[12] for a bead density of $\rho = 3r_c^{-3}$. The soft repulsive interaction parameter a_{ij} between hydrophobic and hydrophilic beads is set at $a_{ij} = 100\ k_bT/r_c$, and is determined by using the Flory-Huggins interaction parameters, χ, as $a_{ij} = a_{ii} + 3.496\chi$, for $\rho = 3r_c^{-3}$.[12]

Model for tyrosine-based block copolymers:

Chemical structure of ABA triblock copolymer, PEG_{5k}-b-oligo(DTO-SA)-b-PEG_{5k}, is shown in Fig. 1(a).[3a, 14a-e] The A blocks are polyethylene glycol (PEG_{5k}) and the B blocks are oligomers of desaminotyrosyl-tyrosine octyl ester (DTO) and suberic acid (SA). A coarse-grained model of a PEG_{5k}-b-oligo(DTO-SA)-b-PEG_{5k} polymer with approximately equal chain lengths of the hydrophobic and hydrophilic blocks was developed to study the initial aggregation. This copolymer encompasses 18 tyrosine-based DTO-SA units as the hydrophobic B block; each DTO-SA unit is represented by a pair of “rigid” (hard) and

Author Manuscript Author Manuscript Author Manuscript Author Manuscript

"flexible" (soft) beads. We derive a flexible bead by coarse-graining the SA group together with the octyl ester group that is originally attached to tyrosine as an "R" group in an amino acid. The remaining DT group is coarse-grained into a rigid bead. This approach results in each bead having an equal molar mass, which is 290 g/mol. The assignment of rigid and flexible beads [see Fig. 1(a)] is based on the chain flexibility of the monomer components due to dissimilarity in their chemical structures. A flexible bead will have more favorable interactions with other flexible beads while a rigid bead will favor interactions with other rigid beads. This can be related to the theory proposed by Putzel and Schick,[19] which suggests that the repulsive interaction between dissimilar lipid molecules (i.e., mixture of saturated and unsaturated lipid molecules) depends on the magnitude of the order parameter. The order parameter is a measure of the degree of order of the saturated lipid chains, in the theory. As the order parameter increases, the repulsive interactions between the saturated and unsaturated lipid molecules will increase, which results in phase segregation of multicomponent lipid membranes. The flexible and rigid units in our model are analogous to the saturated and unsaturated lipid molecules, with the increased soft repulsive interaction parameter between these units reflecting their degree of dissimilarity. The hydrophobic block is linked on either end with an A block comprised of 18 hydrophilic beads with the same molecular weight, as shown in Fig. 1(a). The soft repulsive interaction parameters between the hydrophilic (a), hydrophobic hard (b-h) and soft (b-s), and the solvent (s) beads are shown in Table 1. We would like to note that Groot et al.[12] have provided a detailed discussion on the relationship between the Flory's χ parameter and the DPD interaction parameters. The interaction parameters in our model have been based upon the model introduced by Groot et al. where the interaction parameters between similar species are given by $a_{ii}= 75k_BT/\rho$. ρ is the bead density, which is 3 for this study. The interaction parameter between dissimilar species is given by $a_{ij} = a_{ii} + 3.496\chi$. This relationship between the Flory's χ parameter and the DPD interaction parameters will also hold for our model. For attractive interactions, χ will be negative and for repulsive interactions, χ will be positive. We choose a positive value for χ (for $a_{ij} = 100$) such that microscopic observables from our model are in good agreement with analogous experimental results. We would also like to note that we have not found significant differences in the aggregation characteristics for different values of the soft repulsive interaction parameter $a_{b\text{-}sb\text{-}h}$.

Model for Pluronic® polymers:

The Pluronic® (PEG-PPO-PEG) polymers[13] are modeled by ABA triblock copolymers that are made of segments of hydrophilic and hydrophobic beads, as shown in Fig. 1(b) . We examine four Pluronic® polymers, i.e., F68, F88, F108, and F127, which respectively have an average number of 152.7, 207.3, 265.5, and 200.5 ethylene oxide, and 29.0, 39.3, 50.2, and 65.2 propylene oxide units.[13b] We extend the bead-string model described above to develop a coarse-grained model for Pluronic®. As the inner PPO blocks encompass propylene oxide units only, they were simulated as identical hydrophobic beads. To ensure good comparison with tyrosine-derived polymers, the Pluronic® polymers are modeled as 2 segments of hydrophilic beads, which are connected to a segment of hydrophobic beads. The molar mass of each bead corresponds to 290 g/mol as well (same as tyrosine-derived block copolymer). The B block for F68, F88, F108, and F127 comprises respectively of 6, 8, 11, and 13 hydrophobic beads, whereas the A block encompasses 12, 16, 22 and 15 hydrophilic

Author Manuscript Author Manuscript Author Manuscript Author Manuscript

beads, respectively. The soft repulsive interaction parameters between the hydrophilic (a), hydrophobic (b) and the solvent (s) beads are shown in Table 1.

In our simulations, the respective characteristic length and energy scale are r_c and k_BT. As a result, our characteristic time scale can be described as $\tau = \sqrt{mr_c^2/k_BT}$. Finally, ($\sigma = 3$ and $\Delta t = 0.02\tau$ are used in the simulations along with the total bead number density of $\rho = 3r_c^{-3}$ and a dimensionless value of $r_c = 1$.[18] The mass of all the beads is set to unity.[12,15,18,20]

The characteristic length scale for our model was obtained through the comparison of experimental measurements of the radius of gyration of a PEG_{5K} chain with corresponding measurements using simulations. Experimental measurements of the radius of gyration of PEG_{5K} were found to be 3 nm.[21] A CG model for a PEG_{5K} chain was developed using the same scheme adopted earlier for the typosine-based and Pluronics polymers. The chain was immersed in a hydrophilic solvent and its radius of gyration was measured after the system had equilibrated. The radius of gyration was measured to be 1.4 r_c. A comparison between the experimental and computational results for the radius of gyration yields the length scale for the model, which is given by $r_c = 2.2$ nm. Using a temperature of 37 °C, the energy scale is calculated to be $\varepsilon = k_BT = 4.2\times10^{-21}$ J. The mass of each bead m is assigned to be 290 g/mol. The characteristic time scale for our model was derived by comparing an experimental measurement of the diffusion coefficient of a PEG_{5k} chain in an infinitely dilute solution with a corresponding result obtained from our coarse-grained model, under the same condition. We measured the mean square displacement of the center of mass of the polymer chain and calculated the diffusion coefficient D by the following relation $D = \frac{\left\langle [r(t_0+t) - r(t_0)]^2 \right\rangle}{6t}$, which gives $D = 0.061\, r_c^2/\tau$. Experimental easurements have found the diffusion coefficient for PEG_{5k} in dilute solution to be given by 1.4×10^{-10} m^2/s,[22] which yields a time scale of $\tau = 2.1$ ns.

B. Experimental Methodology

Synthesis of PEG_{5k}-b-oligo(DTO-SA)-b-PEG_{5k} and preparation of tyrospheres: PEG_{5k}-b-oligo(DTO-SA)-b-PEG_{5k} triblock copolymer composed of hydrophilic PEG_{5k} (M.W. 5000 g/mol) blocks and a hydrophobic oligo(DTO-SA) segment was synthesized and characterized as previously reported.[3a, 14c] The degree of polymerization (DP) of oligo(DTO-SA) as determined by ^{1}H-Nuclear Magnetic Resonance (^{1}H-NMR) was 20.4. From this polymer, tyrospheres were prepared as previously reported.[3a, 23]

Determination of the diameter of the micelles by Small Angle X-ray Scattering (SAXS): Tyrospheres were dispersed in pH7.4 PBS buffer as described in our previous publications.[14c] The concentration of the polymer was prepared at a nominal concentration of 25 mg/mL. SAXS data were collected from the as-prepared samples as well as from samples diluted with PBS in the ratio 3:1, 1:1 and 1:3. The hydrodynamic diameters of the tyrospheres were measured by dynamic light scattering, DLS (DelsaNano S, Beckman Coulter Inc., NJ).[3a] X-ray diffraction measurements were carried out in the 5ID-D enclosure in the DND-CAT beam line at the Advance Photon Source, Argonne National Laboratory (Argonne, IL). X-ray beam (wave length, λ = 1.0332 Å) from a Si-(111) double crystal

Author Manuscript Author Manuscript Author Manuscript Author Manuscript

monochromator was collimated with three sets of slits to about 0.2 x 0.2 mm. Small-angle x-ray scattering (SAXS) were collected using 100 x 100 mm Roper camera placed at a distance of 2897 mm from the sample. The tyrosphere dispersions were loaded into 2 mm quartz x-ray capillaries for measurements. Three exposures, each for 2–20 s depending on the concentration, were taken and the data averaged. Scattering curve from the buffer was obtained and subtracted from that of the dispersion.

CAC measurement by pyrene probe method: The CAC of the ABA block copolymer dispersions (PEG_{5k}-b-oligo(DTO-SA)-b-PEG_{5k} and Pluronics®) was determined by a fluorescence technique using pyrene as a fluorescence probe.[8c] When pyrene molecules (final concentration 6x 10^{-6} M) transfer from a hydrophilic to a hydrophobic environment, such as the cores of micellar-like structures of PEG_{5k}-b-oligo(DTO-SA)-b-PEG_{5k}, the (0,0) band in the pyrene excitation spectrum shifts from 334.0–335.0 to 336.5–337.5 nm.[8c] This characteristic feature was utilized to determine the CAC of the ABA triblock copolymer systems.

Fluorescence measurements were carried out on a fluorospectrophotometer (Fluoro-Max2, Long Island Scientific) at room temperature. The pyrene excitation spectra (λ ex = 330 – 340 nm) were monitored at λ em = 393nm. The excitation and emission slit widths were set at 0.5 and 2 nm, respectively; and the spectra were accumulated with an integration time of 3s/nm.

RESULTS AND DISCUSSION

A. Structure and Dynamics of the Self-assembly of ABA Block Copolymers in Aqueous Medium

We examine the aggregation characteristics of the tyrosine-based PEG_{5k}-b-oligo(DTO-SA)-b-PEG_{5k} polymer by studying its self-assembly in solution at a concentration above the experimental reported value of CAC.[24] For the initial setup, we randomly distribute 504 tyrosine-based PEG_{5k}-b-oligo(DTO-SA)-b-PEG_{5k} molecules and solvent beads in a simulation box of dimensions 60 r_c x 60 r_c x 60 r_c, with periodic boundary conditions along the x-, y- and z-axes. The total number of beads in the simulation box is 648000. The unfavorable enthalpic interactions between the hydrophobic and hydrophilic entities drive the aggregation of the molecules to form small clusters that shield the hydrophobic beads from the hydrophilic solvent. A cluster is defined here to encompass 2–4 polymer molecules whose hydrophobic beads are within interaction range; however, the cluster does not possess a spherical core-corona structure. The small clusters diffuse, collide and coalesce in the solvent medium to grow in size to form micelles while simultaneously minimizing the total energy of the system, as shown in Fig. 2. We define micelles to be the equilibrium self-assembled clusters that have a hydrophobic core and a hydrophilic corona (see Fig. 3). The dynamic aggregation process is visualized as animation in Supporting Information (SI) SI. 1. We run the self-assembly simulations for an interval of 50,000 τ until the total energy minimizes to attain an equilibrium value. The aggregation process is characterized through the structure of the aggregates and the aggregation dynamics.

Author Manuscript Author Manuscript Author Manuscript Author Manuscript

An examination of the structure of a micelle demonstrates the presence of a hydrophobic core surrounded by a hydrophilic corona.[3a] The triblock molecules bend at their hydrophobic block to assume a V-shape to accommodate into the hydrophobic region of the micelle, or the micellar core. The dynamic configuration of a single polymer strain in a micelle is shown in SI.2. To verify the shape of individual aggregated polymer molecules in a micelle, we measure the average distance between the center of mass (COM) and the mid-point of the hydrophobic segments of the polymer chains, and compare the results with free polymers. We found the distance from the COM to mid-point for aggregated tyrosine-based polymers ($1.7 \pm 0.4\ r_c$) is larger than that for free polymers ($1.0 \pm 0.3\ r_c$), indicating polymers in micelles possess a V-conformation. The standard deviation is calculated based on deviations due to averaging over time and multiple molecules. Studies have shown the ratio of the hydrophobic to hydrophilic blocks and their relative arrangement to determine the morphology of the self-assembled structures.[25] Control over the architecture of the block copolymers can yield the formation of micelles, polymerosomes, membranes and bicontinuous aggregates. The structure of the micelle is determined by factors responsible for minimizing the free energy of the system. We hypothesize that the bending energy penalty of the individual molecules is compensated by the favorable interactions of the hydrophilic blocks with the solvent. The favorable chain-solvent interactions will result in greater conformational entropy of the hydrophilic segments. Hence, the molecular architecture favors the formation of aggregates with large curvature. We characterize the structure of the micelles by measuring the dimensions of the hydrophobic core and the hydrophilic corona along with the interfacial area per molecule.

Our calculation shows that the micelles have a hydrophobic core with an average diameter of $7.0 \pm 0.7\ r_c$. The dimension of the corona corresponds to the width of the region occupied by the hydrophilic A groups. Calculation of the end-to-end distance of the hydrophilic segments (as shown in Fig. 3) yields an average corona thickness of $4.0 \pm 1.0\ r_c$. The average end-to-end distance of the hydrophilic segments is measured by using Cartesian coordinates of the particles as a function of time obtained from the simulations. This helps track the instantaneous changes in the positions of the particles so that any configuration of the hydrophilic segments during the simulation is taken into account in the measurement of the end-to-end distance. The standard deviation is calculated based on deviations due to averaging over time and multiple molecules. We compute the aggregation number (N_{agg}), which is given by the average number of polymer molecules in a single micelle. For the PEG_{5k}-b-oligo(DTO-SA)-b-PEG_{5k} suspension with 5.6 wt% of polymer, we report the micelles to have an average mass of 271440 g/mol with $N_{agg} = 13$. Combining the thickness of the corona and the size of the hydrophobic core, our simulations yield an average geometric diameter of $15.0 \pm 2.0\ r_c$. We also measure the interfacial area per molecule by dividing the surface area of the aggregate with the total number of polymer molecules present in the aggregate. The surface area is obtained by representing the aggregate as a sphere, as shown in Fig. 3. The interfacial area per molecule is found to be $40.0 \pm 1.0\ r_c^2$ by considering both corona and hydrophobic core, and $9.62 \pm 0.07\ r_c^2$ by only considering the hydrophobic core. We also conduct size measurements for micelles encompassing tyrosine-based ABA copolymer with DP of the oligo(DTO-SA) group to be given by 4, 8 and 18, as

Author Manuscript Author Manuscript Author Manuscript Author Manuscript

shown in Table 1. As expected, we observe the micellar core to increase in dimension with the DP.

To verify the size measurement by simulation method, we synthesized a PEG_{5k}-oligo(DTO-SA)-b-PEG_{5k} block copolymer (DP of DTO-SA = 20.4) and prepared tyrospheres. The hydrodynamic diameter of the nanospheres determined from DLS was 68.5 nm at 16 mg/mL and 64.9 nm at 0.16 mg/mL. The geometric size of the spheres was determined from the SAXS data. The background subtracted data were used to obtain Guinier plots, Ln(I) vs. q^2 plots, where I is the scattered intensity and q is the scattering vector (= $4\pi\sin(\theta)/\lambda$, 2θ is the scattering angle).[26] Fig. 4 shows an example of the data. Similar plots were obtained from all the samples. Clearly, the plot shows two linear regions. These regions were used to obtain two radii of gyration (R_g) from the equation $I(q) = I(0)\exp(-q^2 R_g^2/3)$ from the slopes of the Ln(I) vs. q^2 curve. The average R^2 of the fitted lines for the low- and the high-angle regions were respectively 0.997 and 0.971, indicating the nanospheres are highly monodisperse with regard to both the sizes. The R_g were used to obtain the diameters assuming spherical shape for the scattering particle ($D=2*R_g*\sqrt{(5/3)}$). The diameters calculated from both the slopes did not change significantly with dilution. The micellar diameter calculated from the slope of the low-angle region ($2 < q^2*10^4$ Å$^{-2}< 8$) was 33.24 ± 0.11 nm which is close to the micelle diameter of the polymer with DP = 18 (33 ± 6 nm, see Table 1) as determined from simulations. The micellar diameter is about half the hydrodynamic diameter showing that the hydration effects of PEG to extend beyond the corona. The core diameter calculated from the slope of the high-angle region ($20 < q^2*10^4$ Å$^{-2} < 60$) was 9.4 ± 0.3 nm. The SAXS core diameter is determined by the difference in electron density between the core and the corona, and hence underestimates the actual diameter. It is possible that the distribution of the hydrophobic segments decreases from the center of the core towards the corona. Thus, the size of the core as defined by the hydrophobicity (impermeable to water) could be larger than that defined by the electron density.

We characterize the aggregation dynamics by computing the time evolution of the number of clusters and the size of the clusters,[11a,12,27] as shown in Fig. 5. At early times ($0 < t < 1340\ \tau$) during the aggregation process, we observe the polymer molecules to diffuse in the solvent medium, collide and coalesce to form small clusters. At later times ($t > 1340\ \tau$), the small clusters diffuse, collide and coalesce to form micelles. Our measurements show that the aggregation process slows down with the formation of small clusters on account of the hydrodynamic drag due to the favorable interactions of the A blocks with the solvent. An additional contribution arises from the stabilization of the cluster interface due to steric hindrance promoted by the hydrophilic chains. We would like to note that the time evolution of the aggregation characteristics reaches equilibrium during the interval of the simulation.

The time evolution of the aggregation dynamics can be used to compute the scaling exponent of the clustering process by using the following relation $N(t) \sim C\, t^{-\alpha}$, where $N(t)$ is the number of clusters, C is a constant, t is time, and α is the scaling exponent. Similarly, the growth in the average size of a cluster can be characterized by using the following relation $\langle S(t) \rangle \sim D\, t^{\beta}$, where $\langle S(t) \rangle$ is the average size of the clusters, D is a constant, and β is the scaling exponent. The dynamics of the clustering process is shown in Fig. 5. The average cluster size effectively provides the volume occupied by the non-solvent beads in a cluster as

Author Manuscript Author Manuscript Author Manuscript Author Manuscript

the density in the system is constant. The average linear size of the cluster becomes $R(t) \sim (< S(t) >)^{1/3} \sim (t^{\beta})^{1/3} \sim t^{0.06}$. Based on the growth dynamics, we determine that $\alpha = -0.19 \pm 0.01$ and $\beta = 0.19 \pm 0.01$. Previous studies show the growth dynamics of the clusters to be affected by the length of hydrophilic blocks in the molecule, which have favorable enthalpic interactions with the solvent.[15a, 28] As a consequence, molecules with longer hydrophilic groups have slower aggregation dynamics. The resulting decrease in the magnitude of the scaling exponents with the length of hydrophilic blocks as reported in previous studies[15a, 28] supports our findings. We would like to note that the scaling exponents have been calculated based upon particle trajectories from four simulations with identical initial particle spatial configurations but different initial particle velocities.

We use an identical protocol to the one adopted for the PEG_{5k}-b-oligo(DTO-SA)-b-PEG_{5k} triblock copolymer to examine the self-assembly of Pluronic® F127. We use a simulation box of dimensions 60 r_c x 60 r_c x 60 r_c with 504 molecules (5.6 wt%) randomly dispersed along with the solvent beads. We allow the self-assembly process to run for a time interval of 50,000τ which is very similar to that observed for the PEG_{5k}-b-oligo(DTO-SA)-b-PEG_{5k} triblock copolymer, as shown in Fig. 6. The aggregation process for Pluronic® F127 is also visualized as animation in Supporting Information (SI) SI.3. The time evolution of the aggregation dynamics of Pluronic® F127 is shown in Fig. 7. We determined the aggregation dynamics scaling exponent to be $\alpha = -0.18 \pm 0.03$ and $\beta = 0.18 \pm 0.03$. We note that experimental measurements of the average hydrophobic core sizes of Pluronic® F127 micelles (in aqueous solution) report values of 6.0 nm and 10.8 nm, respectively for 5 wt% and 10 wt% of polymer.[29] Simulations examining micelle core sizes for systems with 5 wt% and 10 wt% of the F127 polymer, report diameters of 3.6 ±0.8 r_c and 4.0 ± 0.6 r_c, respectively (corresponding to 8.0 ± 2.0 nm and 9.0 ± 1.0 nm). Clearly, the micelle core size values determined from simulations agreed well with experimental data as reported in literature. These results demonstrate the coarse-grained model to capture both structural and dynamical characteristics of Pluronic® ABA copolymers.

B. CAC of ABA Block Copolymers in Aqueous Medium: Prediction of CAC and Validation of Coarse-Grained Model Using Pyrene Probe Method

CAC of a polymeric self-assembling system reflects the lowest polymer concentration that generates aggregates. CAC is the key parameter for clinical application of nano-sized drug carriers, since it determines whether the drug carriers will be stable or dissociate *in vivo* when diluted upon injection. CAC of self-assembled systems can be determined via experimental methods such as static light scattering, pyrene method, and surface tension measurement.[8] It is noted in literature that for the same drug delivery system, CAC values determined by different methods can vary by factors of 3 – 10.[30] CAC values can also be determined through computational approaches.[11b, 27b, 31] A unique advantage of the computational route is the ability to determine CAC values of drug delivery systems based on a virtual library of numerous ABA block polymers. This has a distinct advantage (in comparison to corresponding results from the experimental approach) of being more cost and time effective. However, computational prediction of the CAC requires a model that has been validated and refined to capture the chemistry of the polymer. Hence, we will use the model to predict the CAC for Pluronic® polymers F68, F88, F108, and F127, and the

Author Manuscript Author Manuscript Author Manuscript Author Manuscript

PEG_{5k}-b-oligo(DTO-SA)-b-PEG_{5k} polymer. The comparison between predicted and experimentally determined values of CAC for these polymers will validate the model and the coarse-graining scheme.

Via the DPD simulation technique, CAC values for Pluronic® polymers F68, F88, F108, and F127 were determined by randomly placing a given number of polymer molecules along with solvent beads in a simulation box. Each simulation was run for a fixed time interval spanning 20,000 τ. If a given polymer concentration demonstrates aggregation, we reduce the concentration, rerun the simulation and test for aggregation. We repeat this process until we reach a concentration at which we just begin to observe aggregation. The corresponding concentration is called the CAC. We compared CAC values obtained using the coarse-grained models for these polymers with corresponding experimental measurements by the pyrene method, as reported in Table 2. The computational and experimental CAC values are in excellent agreement: the experimental values are about 1.3 to 3.2 fold of the values determined by simulation. Moreover, the CAC values of Pluronics® have been well reported in literature,[32] and are in good agreement with our experimental and simulation results (see Table 2). These results demonstrate the proof-of-concept for the combined computational-experimental approach to predict aggregation characteristics of ABA block copolymers.

We would like to note that the agreement between CAC values obtained using computational and experimental approaches significantly improves for Pluronics ABA triblock copolymers with lower CAC values. The CAC value of a polymer is determined by the lengths of its hydrophilic A and hydrophobic B blocks. The unfavorable enthalpic interactions between the hydrophobic B blocks and the hydrophilic solvent drive the aggregation of the polymer chains. However, the solubility, conformational entropy and steric hindrance of the hydrophilic A blocks along with the configurational entropy of the polymer chains counters the aggregation process. The assembly arising from the minimization of the system free energy will occur when the unfavorable enthalpic interactions between hydrophilic and hydrophobic components outweighs the other factors. We surmise that our Pluronics model is highly effective in capturing the unfavorable enthalpic interactions between the hydrophobic B blocks and the hydrophilic solvent. Hence, we are able to reproduce the CAC values of polymers with large hydrophobic B blocks with a fair degree of accuracy. For polymers with high CAC, the conformational entropy and steric hindrance of the A blocks outweighs the unfavorable enthalpic interactions between the hydrophobic B block and the hydrophilic solvent; hence, the incipience of aggregation for these polymers occurs at higher concentrations. Our current model for Pluronics needs further refinement to be able to capture the effects of steric hindrance and conformational entropy of the A blocks in Pluronics ABA triblock copolymers with high CAC.

We assessed whether the coarse-grained model was able to accurately capture the CAC values for a more complex block copolymer such as PEG_{5k}-b-oligo(DTO-SA)-b-PEG_{5k}. It is computationally prohibitively expensive to determine the CAC of PEG_{5k}-b-oligo(DTO-SA)-b-PEG_{5k} with a high molecular weight and hence, long hydrophobic B block. Therefore, we adopt an alternate approach introduced by an earlier study to predict the CAC value for a diblock polymer with a relatively long hydrophobic block. This method used CAC measurements for a series of diblock polymers with shorter hydrophobic blocks while

Author Manuscript Author Manuscript Author Manuscript Author Manuscript

maintaining constant the length of the hydrophilic block to extrapolate the CAC value of the diblock with the desired length of the hydrophobic block.[33] To simplify the computation, a series of tyrosine-derived polymers with fixed hydrophilic chain length (M.W. of PEG_{5k} = 5000 g/mol) and variable hydrophobic segment length of chemical structure DTO-SA were used. We construct five different tyrosine-based polyarylate-$PEG_{\mathbf{5k}}$ polymers with the same length of the PEG block (5000 g/mol) as in the original model (18 hydrophilic beads per PEG_{5k} segment, as shown in Fig. 1a), but with 3, 4, 5, 6 and 8 pairs of hard and soft hydrophobic beads. The CAC values for these five different tyrosine-based polyarylate-$PEG_{\mathbf{5k}}$ polymers is determined using the simulation protocol detailed earlier, and are used to predict the CAC corresponding to a tyrosine-based polyarylate-$PEG_{\mathbf{5k}}$ polymer with the same length of the PEG block (5000 g/mol) but with 18 pairs of hard and soft beads (DP ~ 20). In parallel, a tyrosine-derived polymer with DP value of 20.4 was synthesized and its CAC value was determined via the pyrene method.[8c] The computational and experimental data are in good agreement with each other: the experimentally determined CAC value for PEG_{5k}-b-oligo(DTO-SA)-b-PEG_{5k} copolymer is close to the corresponding computational measurement (see Fig. 8). This result validates the model and demonstrates its potential to predict aggregation characteristics of the tyrosine-based copolymers.

CONCLUSIONS

In this study, we proposed a coarse-grained model for ABA tri-block copolymers including Pluronics® and PEG_{5k}-b-oligo(DTO-SA)-b-PEG_{5k}. We investigated the aggregation dynamics for both Pluronics® and PEG_{5k}-b-oligo(DTO-SA)-b-PEG_{5k} during the self-assembly process. In the early stages of the self-assembly process, the polymer molecules formed small clusters via diffusion, collision and coalescence. The small clusters collided and coalesced further to form polymer micelles in the later stages. The morphology of micelles was determined to be core-corona structures with individual polymers bending into V-shape to form hydrophobic core and hydrophilic corona. Size measurements on the micelle core and corona were conducted for PEG_{5k}-b-oligo(DTO-SA)-b-PEG_{5k} with DP =18, and for Pluronic® F127, and were found to be in good agreement with corresponding results obtained via experiments.

The model is also used to determine the CAC values of Pluronics® and PEG_{5k}-b-oligo(DTO-SA)-b-PEG_{5k} micelles. Our simulation results for the CAC for Pluronics® and PEG_{5k}-b-oligo(DTO-SA)-b-PEG_{5k} are found to be in a reasonably good agreement with the experimental measurements. These results demonstrated experimental validation of our computational model and method on the self-assembly of ABA copolymers.

Our results can be used to determine structural and dynamical properties of polymer based drug delivery systems and build a virtual library of numerous ABA block polymers. These libraries can be utilized to optimize the design of drug delivery systems by simulating the interactions between ABA block copolymers and various drug molecules, and predict their drug encapsulation and release features.

Author Manuscript Author Manuscript Author Manuscript Author Manuscript

Supplementary Material

Refer to Web version on PubMed Central for supplementary material.

ACKNOWLEDGEMENTS

The authors would like to acknowledge Professor S. Sofou and C. Zhu for assistance in fluorescent spectrometry measurement. Portion of the research was supported by RESBIO - The National Resource for Polymeric Biomaterials supported by the National Institutes of Health (NIH grant EBOO1046), and by the New Jersey Center for Biomaterials. The X-ray scattering work was carried out on the beam line 5ID-D at the Advanced Photon Source (APS), Argonne National Laboratory, which is funded by Department of Energy. We would like to acknowledge Dr. Steven Weigand at the APS for enabling the X-ray data measurements. The authors would like to acknowledge the use of high performance computational resources at the Rutgers Discovery Informatics Institute (http://rdi2.rutgers.edu/). Portions of the research were also conducted using high performance computational resources provided by Extreme Science and Engineering Discovery Environment (XSEDE) at the Texas Advanced Computing Center and the San Diego Supercomputing Center through allocations TG-DMR140099, TG-DMR140125, TG-DMR110109, TG-DMR140060 and TG-MCB090174.

Glossary of abbreviations:

CAC:
Critical Aggregation Concentration

CG:
Coarse-grained

DLS:
dynamic light scattering

DP:
degree of polymerization

DPD:
Dissipative Particle Dynamics

DTO:
Desaminotyrosyl-tyrosine octyl ester

EO:
Ethylene oxide

MD:
Molecular Dynamics

M.W.:
Molecular Weight

NMR:
Nuclear Magnetic Resonance

PBS:
Phosphate Buffered Saline

Author Manuscript Author Manuscript Author Manuscript Author Manuscript

PEG:
Poly(ethylene glycol)

PEG_{5k}:
Poly(ethylene glycol), molecular weight = 5000 g/mol

PEG_{5K}-b-oligo(DTO-SA)-b-PEG_{5K}:
PEG_{5K}-*b*-oligo(desaminotyrosyl-tyrosine octyl ester-suberate)-*b*-PEG_{5K}

PO:
Propylene oxide

PPO:
Poly(propylene oxide)

SA:
Suberic acid

SAXS:
Small Angle X-ray Scattering

Tyrosphere(s):
Tyrosine-derived nanosphere(s)

REFERENCES CITED

1. Yan L; Yang Y; Zhang WJ; Chen XF, Advanced Materials and Nanotechnology for Drug Delivery. Adv Mater 2014, 26 (31), 5533–5540. [PubMed: 24449177]
2. (a)Liu CH; Liu RH; Sun QJ; Chang JB; Gao X; Liu Y; Lee ST; Kang ZH; Wang SD, Controlled synthesis and synergistic effects of graphene-supported PdAu bimetallic nanoparticles with tunable catalytic properties. Nanoscale 2015, 7 (14), 6356–6362; [PubMed: 25786139] (b)Felice B; Prabhakaran MP; Rodriguez AP; Ramakrishna S, Drug delivery vehicles on a nano-engineering perspective. Mat Sci Eng C-Mater 2014, 41,178–195.
3. (a)Sheihet L; Piotrowska K; Dubin RA; Kohn J; Devore D, Effect of tyrosine-derived triblock copolymer compositions on nanosphere self-assembly and drug delivery. Biomacromolecules 2007, 8 (3), 998–1003; [PubMed: 17274654] (b)Sun LM; Fan Z; Wang YZ; Huang YJ; Schmidt M; Zhang MJ, Tunable synthesis of self-assembled cyclic peptide nanotubes and nanoparticles. Soft Matter 2015, 11 (19), 3822–3832. [PubMed: 25858105]
4. Torchilin VP, Structure and design of polymeric surfactant-based drug delivery systems. J Control Release 2001, 73 (2–3), 137–172. [PubMed: 11516494]
5. Allen C; Maysinger D; Eisenberg A, Nano-engineering block copolymer aggregates for drug delivery. Colloid Surface B 1999,16 (1–4), 3–27.
6. (a)Torchilin VP, Micellar nanocarriers: Pharmaceutical perspectives. Pharm Res 2007, 24 (1), 1–16; [PubMed: 17109211] (b)Nam YS; Kang HS; Park JY; Park TG; Han SH; Chang IS, New micelle-like polymer aggregates made from PEI-PLGA diblock copolymers: micellar characteristics and cellular uptake. Biomaterials 2003, 24 (12), 2053–2059. [PubMed: 12628825]
7. Du HB; Zhu JT; Jiang W, Study of controllable aggregation morphology of ABA amphiphilic triblock copolymer in dilute solution by changing the solvent property. J Phys Chem B 2007, 111 (8), 1938–1945. [PubMed: 17274648]
8. (a)Gracia CA; Gomez-Barreiro S; Gonzalez-Perez A; Nimo J; Rodriguez JR, Static and dynamic light-scattering studies on micellar solutions of alkyldimethylbenzylammonium chlorides. J Colloid Interf Sci 2004, 276 (2), 408–413;(b)Lin SY; Lin YY; Chen EM; Hsu CT; Kwan CC, A study of the

Author Manuscript Author Manuscript Author Manuscript Author Manuscript

equilibrium surface tension and the critical micelle concentration of mixed surfactant solutions. Langmuir 1999, 15 (13), 4370–4376,(c)Zhang Z; Grijpma DW; Feijen J, Thermo-sensitive transition of monomethoxy poly(ethylene glycol)-block-poly(trimethylene carbonate) films to micellar-like nanoparticles. J Control Release 2006, 112 (1), 57–63. [PubMed: 16516326]

9. Wijmans CM; Eiser E; Frenkel D, Simulation study of intra- and intermicellar ordering in triblock-copolymer systems. J Chem Phys 2004, 120 (12), 5839–5848. [PubMed: 15267463]
10. Chen T; Hynninen AP; Prud'homme RK; Kevrekidis IG; Panagiotopoulos AZ, Coarse-Grained Simulations of Rapid Assembly Kinetics for Polystyrene-b-poly(ethylene oxide) Copolymers in Aqueous Solutions. J Phys Chem B 2008, 112 (51), 16357–16366. [PubMed: 19367859]
11. (a)Spaeth JR; Kevrekidis IG; Panagiotopoulos AZ, A comparison of implicit- and explicit-solvent simulations of self-assembly in block copolymer and solute systems. J Chem Phys 2011, 134 (16); (b)Li ZL; Dormidontova EE, Kinetics of Diblock Copolymer Micellization by Dissipative Particle Dynamics. Macromolecules 2010, 43 (7), 3521–3531.
12. Groot RD; Warren PB, Dissipative particle dynamics: Bridging the gap between atomistic and mesoscopic simulation. J Chem Phys 1997, 107 (11), 4423–4435.
13. (a)Kabanov AV; Nazarova IR; Astafieva IV; Batrakova EV; Alakhov VY; Yaroslavov AA; Kabanov VA, Micelle Formation and Solubilization of Fluorescent-Probes in Poly(Oxyethylene-B-Oxypropylene-B-Oxyethylene) Solutions. Macromolecules 1995, 28 (7), 2303–2314;(b)Kabanov AV;Batrakova EV; Alakhov VY, Pluronic (R) block copolymers as novel polymer therapeutics for drug and gene delivery. J Control Release 2002, 82 (2–3), 189–212. [PubMed: 12175737]
14. (a)Kilfoyle BE; Sheihet L; Zhang Z; Laohoo M; Kohn J; Michniak-Kohn BB, Development of paclitaxel-TyroSpheres for topical skin treatment. J Control Release 2012, 163 (1), 18–24; [PubMed: 22732474] (b)Bushman J; Vaughan A; Sheihet L; Zhang Z; Costache M; Kohn J, Functionalized nanospheres for targeted delivery of paclitaxel. J Control Release 2013, 171 (3), 315–321; [PubMed: 23792807] (c)Sheihet L; Dubin RA; Devore D; Kohn J, Hydrophobic drug delivery by self-assembling triblock copolymer-derived nanospheres. Biomacromolecules 2005, 6 (5), 2726–31; [PubMed: 16153112] (d)Costache AD; Sheihet L; Zaveri K; Knight DD; Kohn J, Polymer-Drug Interactions in Tyrosine-Derived Triblock Copolymer Nanospheres: A Computational Modeling Approach. Mol Pharmaceut 2009, 6 (5), 1620–1627;(e)Zhang Z; Tsai PC; Ramezanli T; Michniak-Kohn BB, Polymeric nanoparticles-based topical delivery systems for the treatment of dermatological diseases. Wires Nanomed Nanobi 2013, 5 (3), 205–218;(f)Goyal R; Macri L; Kohn J, Formulation Strategy for the Delivery of Cyclosporine A: Comparison of Two Polymeric Nanospheres. Scientific reports 2015, 5,13065. [PubMed: 26268451]
15. (a)Dutt M; Kuksenok O; Nayhouse MJ; Little SR; Balazs AC, Modeling the Self-Assembly of Lipids and Nanotubes in Solution: Forming Vesicles and Bicelles with Transmembrane Nanotube Channels. Acs Nano 2011, 5 (6), 4769–4782; [PubMed: 21604769] (b)Aydin F; Ludford P; Dutt M, Phase segregation in bio-inspired multi-component vesicles encompassing double tail phospholipid species. Soft Matter 2014, 10 (32), 6096–108. [PubMed: 25008809]
16. Allen MPT, D. J., Computer Simulations of Liquids. Clarendon Press: Oxford, 2001.
17. Plimpton S, Fast Parallel Algorithms for Short-Range Molecular-Dynamics. J Comput Phys 1995, 117 (1), 1–19.
18. Smith KA; Jasnow D; Balazs AC, Designing synthetic vesicles that engulf nanoscopic particles. J Chem Phys 2007, 127 (8).
19. Putzel GG; Schick M, Phenomenological Model and Phase Behavior of Saturated and Unsaturated Lipids and Cholesterol. Biophys J 2008, 95 (10), 4756–4762. [PubMed: 18708463]
20. (a)Iliya G; Lipowsky R; Shillcock JC, Two-component membrane material properties and domain formation from dissipative particle dynamics. J Chem Phys 2006, 125 (11), 114710; [PubMed: 16999504] (b)Kranenburg M; Venturoli M; Smit B, Phase behavior and induced interdigitation in bilayers studied with dissipative particle dynamics. J Phys Chem B 2003, 107 (41), 11491–11501.
21. Devanand K; Selser JC, Asymptotic-Behavior and Long-Range Interactions in Aqueous-Solutions of Poly(Ethylene Oxide). Macromolecules 1991, 24 (22), 5943–5947.
22. Johansson L; Skantze U; Lofroth JE, Diffusion and Interaction in Gels and Solutions .2. Experimental Results on the Obstruction Effect. Macromolecules 1991, 24 (22), 6019–6023.
23. Sheihet L; Garbuzenko OB; Bushman J; Gounder MK; Minko T; Kohn J, Paclitaxel in tyrosine-derived nanospheres as a potential anti-cancer agent: In vivo evaluation of toxicity and efficacy in

Author Manuscript Author Manuscript Author Manuscript Author Manuscript

comparison with paclitaxel in Cremophor. EurJ Pharm Sci 2012, 45 (3), 320–329. [PubMed: 22155544]

24. Nardin C; Bolikal D; Kohn J, Nontoxic block copolymer nanospheres: design and characterization. Langmuir 2004, 20 (26), 11721–5. [PubMed: 15595803]
25. (a)Jain S; Bates FS, On the origins of morphological complexity in block copolymer surfactants. Science 2003, 300 (5618), 460–464; [PubMed: 12702869] (b)Srinivas G; Discher DE; Klein ML, Self-assembly and properties of diblock copolymers by coarse-grain molecular dynamics. Nat Mater 2004, 3 (9), 638–644. [PubMed: 15300242]
26. Guinier A; Fournet G, Small angle scattering of X-rays. J. Wiley & Sons, New York 1955.
27. (a)Aydin F; Dutt M, Bioinspired Vesicles Encompassing Two-Tail Phospholipids: Self-Assembly and Phase Segregation via Implicit Solvent Coarse-Grained Molecular Dynamics. J Phys Chem B 2014, 118 (29), 8614–8623; [PubMed: 24987793] (b)Vishnyakov A; Lee MT; Neimark AV, Prediction of the Critical Micelle Concentration of Nonionic Surfactants by Dissipative Particle Dynamics Simulations. J Phys Chem Lett 2013, 4 (5), 797–802. [PubMed: 26281935]
28. Aydin F; Uppaladadium G; Dutt M, The design of shape-tunable hairy vesicles. Colloids and surfaces. B, Biointerfaces 2015, 128, 268–75. [PubMed: 25701116]
29. Lam YM; Grigorieff N; Goldbeck-Wood G, Direct visualisation of micelles of Pluronic block copolymers in aqueous solution by cryo-TEM. Phys Chem Chem Phys 1999, 1 (14), 3331–3334.
30. (a)Lee K; Shin SC; Oh I, Fluorescence spectroscopy studies on micellization of poloxamer 407 solution. Archives of pharmacal research 2003, 26 (8), 653–8; [PubMed: 12967202] (b)Li X; Mya KY; Ni X; He C; Leong KW; Li J, Dynamic and static light scattering studies on self-aggregation behavior of biodegradable amphiphilic poly(ethylene oxide)-poly[(R)-3-hydroxybutyrate]-poly(ethylene oxide) triblock copolymers in aqueous solution. J Phys Chem B 2006, 110 (12), 5920–6; [PubMed: 16553399] (c)Zhu C; Pang S; Xu J; Jia L; Xu F; Mei J; Qin A; Sun J; Ji J; Tang B, Aggregation-induced emission of tetraphenylethene derivative as a fluorescence method for probing the assembling/disassembling of amphiphilic molecules. The Analyst 2011, 136 (16), 3343–8. [PubMed: 21750804]
31. (a)Sanders SA; Panagiotopoulos AZ, Micellization behavior of coarse grained surfactant models. J Chem Phys 2010, 132 (11), 114902; [PubMed: 20331315] (b)Burov SV; Vanin AA; Brodskaya EN, Principal role of the stepwise aggregation mechanism in ionic surfactant solutions near the critical micelle concentration. Molecular dynamics study. J Phys Chem B 2009, 113 (31), 10715–20; [PubMed: 19591445] (c)Stephenson BC; Beers K; Blankschtein D, Complementary use of simulations and molecular-thermodynamic theory to model micellization. Langmuir 2006, 22 (4), 1500–13; [PubMed: 16460068] (d)Yang S; Zhang X; Yuan S, Mesoscopic simulation studies on micellar phases of Pluronic P103 solution. Journal of molecular modeling 2008, 14 (7), 607–20. [PubMed: 18478279]
32. (a)Samith VD; Mino G; Ramos-Moore E; Arancibia-Miranda N, Effects of pluronic F68 micellization on the viability of neuronal cells in culture. J Appl Polym Sci 2013, 130 (3), 2159–2164;(b)Nakashima K; Anzai T; Fujimoto Y, Fluorescence Studies on the Properties of a Pluronic F68 Micelle. Langmuir 1994, 10 (3), 658–661;(c)Alexandridis P; Holzwarth JF; Hatton TA, Micellization of Poly(Ethylene Oxide)-Poly(Propylene Oxide)-Poly(Ethylene Oxide) Triblock Copolymers in Aqueous-Solutions - Thermodynamics of Copolymer Association. Macromolecules 1994, 27 (9), 2414–2425.
33. Kenjiro Meguro YT, Kawahashi Nobuo, Tabata Yujin, Ueno Minoru, Micellar properties of a series of octaethyleneglycol-n-alkyl ethers with homogeneous ethylene oxide chain and their temperature dependence. J Colloid Interf Sci 1981, 83 (1), 50–56.

Author Manuscript Author Manuscript Author Manuscript Author Manuscript

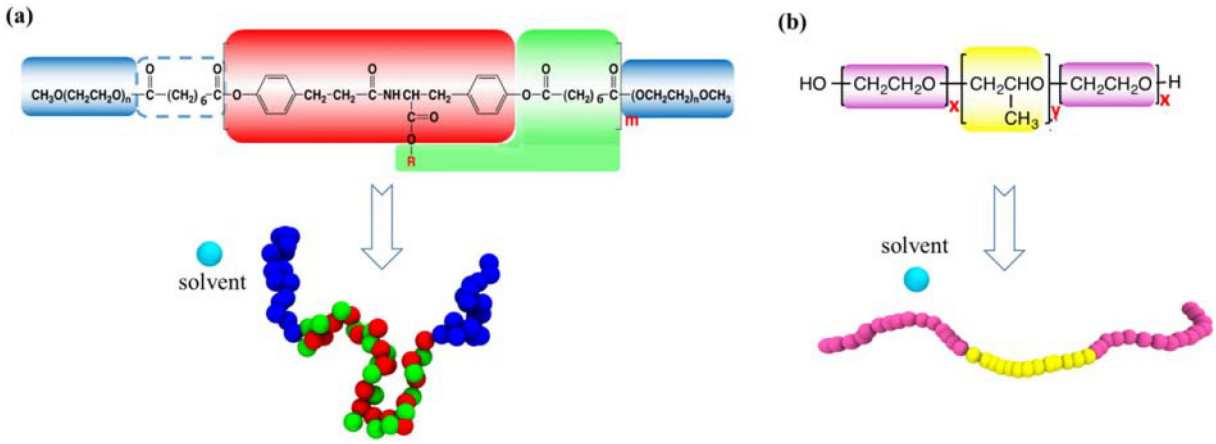

Figure 1:

Schematics of coarse-graining (a) PEG_{5k}-b-oligo(DTO-SA)-b-PEG_{5k}, and (b) Pluronic® block polymers, (a) For PEG_{5K}-b-oligo(DTO-SA)-b-PEG_{5K}, the hydrophilic PEG_{5K} moieties on each end of the polymer are modeled with 18 beads (blue). The group in dashed line is nonrepeated conjunct group which only affects one coarse-graining site. Each repeating unit (DTO-SA) in the hydrophobic B block is divided into a hard section (desaminotyrosyl tyrosine) and a soft section (suberic acid and pendent octyl chain), which are respectively coarse-grained into red and green beads. The entire B block is modeled with 18 pairs of hard (red) and soft (green) beads, (b) Pluronic® F68 has A blocks that encompass 12 hydrophilic beads (magenta), each corresponding to roughly 6.6 EO units, and a B block that includes 6 hydrophobic beads (yellow), each corresponding to 5 PO units. The molar mass of each bead is 290 g/mol.

Author Manuscript Author Manuscript Author Manuscript Author Manuscript

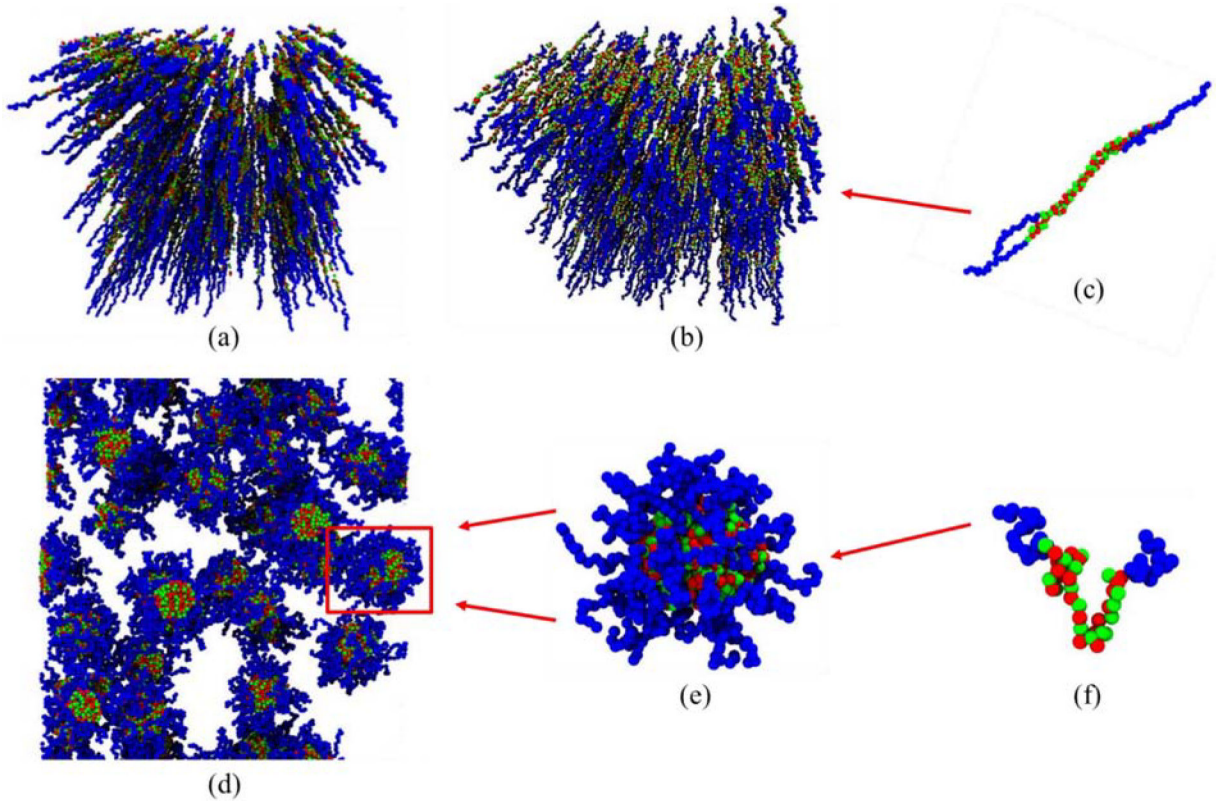

Figure 2:

(a) Initial system configuration (t = 0 **τ**) with 504 copolymers arranged so that there is no intermolecular interaction between any two individual molecules, simulation box size is $60r_c \times 60r_c \times 60r_c$. (b) System snapshot at t = 20 **τ**, when polymers starts to form small clusters, (c) A single cluster of two polymer molecules captured among many clusters formed at t = 20 **τ**, (d) Snapshot of the system t = 50,000 **τ**. (e) Magnified image of a single micelle in the system, (f) An individual polymer molecule in a micelle bends into V-shape structure.

Author Manuscript Author Manuscript Author Manuscript Author Manuscript

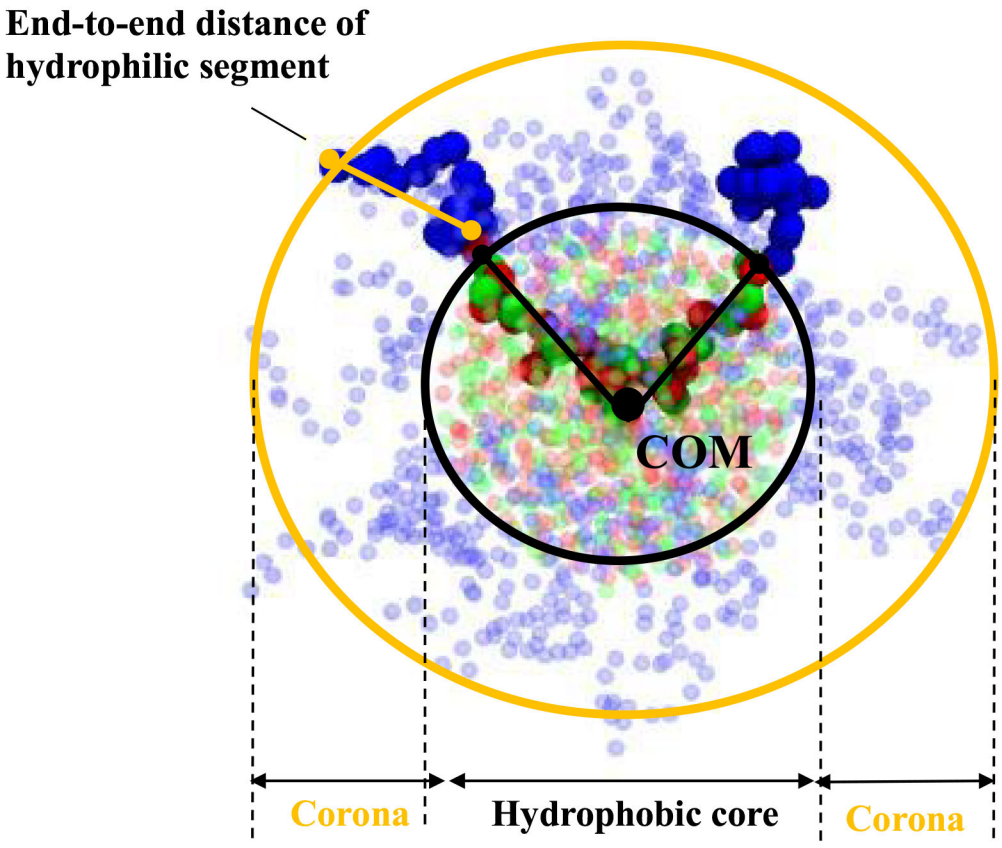

Figure 3:

Core-corona structure of a micelle obtained in the system with 504 copolymers as shown in Fig. 2. Size of hydrophobic core (black circle) is evaluated by measuring distance from center of mass (COM) of a micelle to the end beads of hydrophobic segment averaged over all “hydrophobic segments”. Corona is measured by calculating end-to-end distance of hydrophilic segment averaged over all “hydrophilic segments”.

Author Manuscript Author Manuscript Author Manuscript Author Manuscript

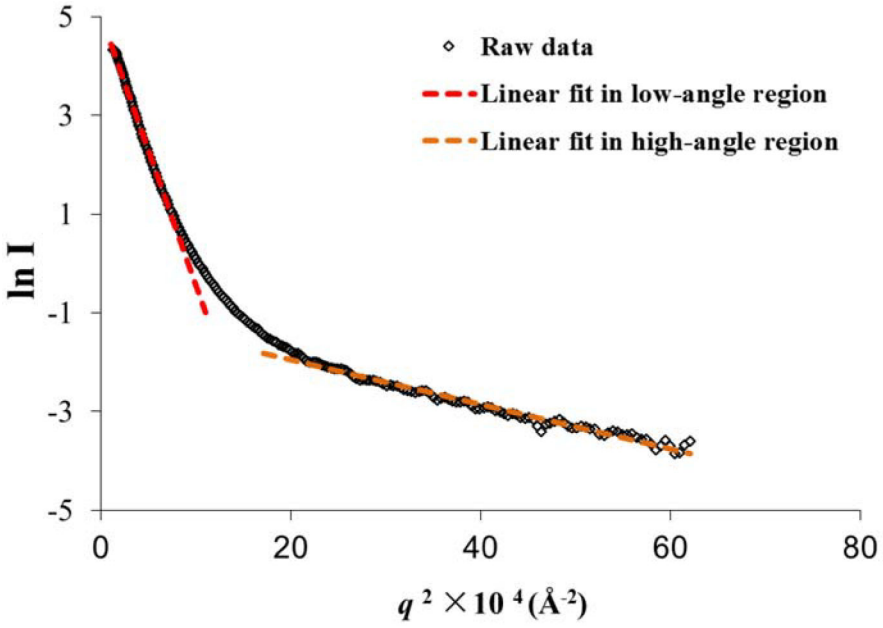

Figure 4:

Guinier plot of SAXS data. Dashed lines are the separate fits to the low- and high-angle region of the raw data using the Guinier equation ($I(q) = I(0) \exp(-q^2 R_g^2/3)$).

Author Manuscript Author Manuscript Author Manuscript Author Manuscript

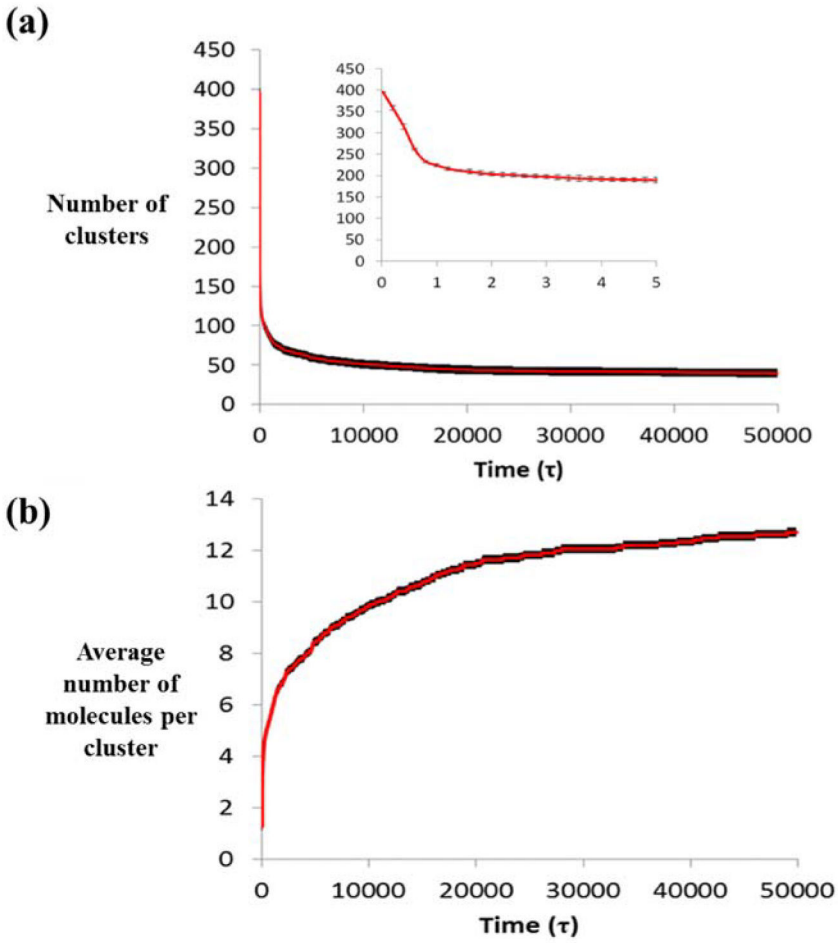

Figure 5:

Time evolution of (a) the number of clusters and (b) the average cluster size (that is, number of molecules) for a system with 504 copolymers as shown in Figure 2. The inset in panel (a) shows the numbers of clusters from time 0 to 5τ.

Author Manuscript Author Manuscript Author Manuscript Author Manuscript

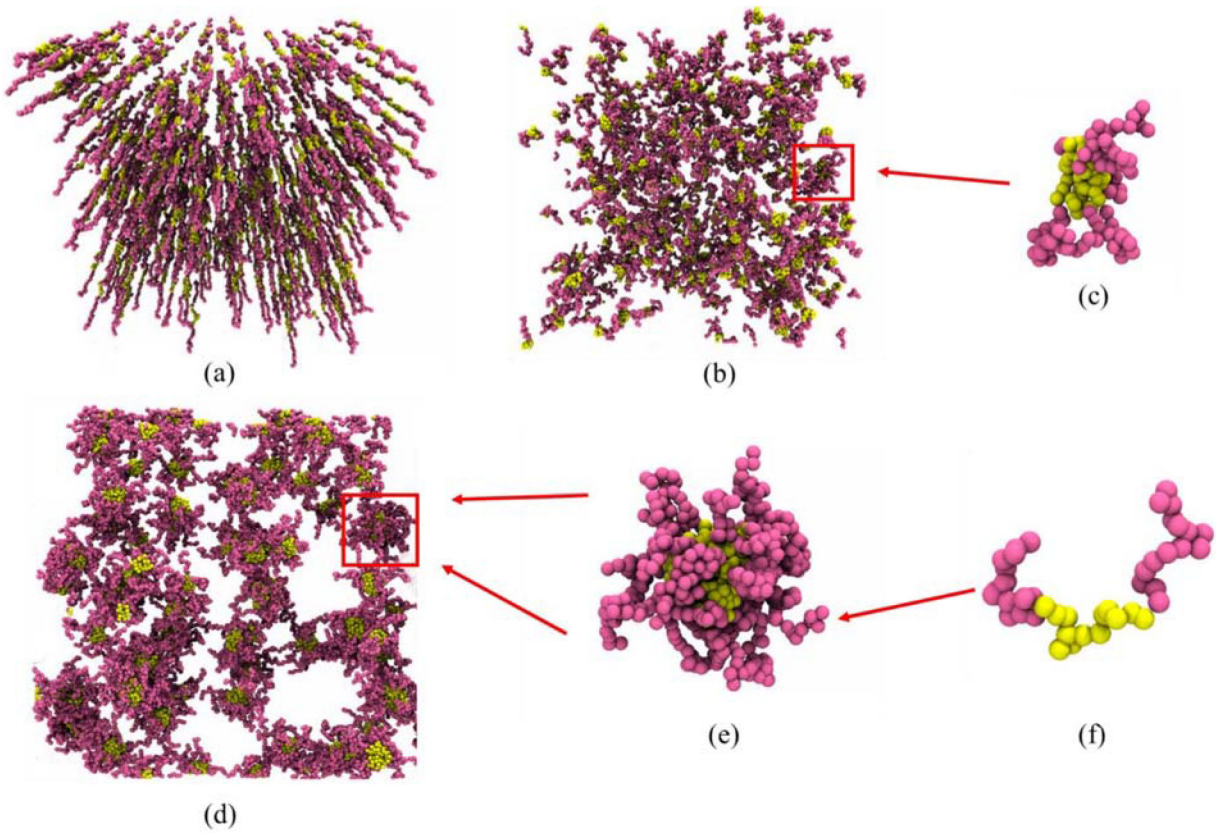

Figure 6:

(a) Initial system configuration (t = 0 **τ**) with 504 Pluronic® F127 arranged so that there is no intermolecular interaction between any two individual molecules. The simulation box size is $60r_c \times 60r_c \times 60r_c$. (b) System snapshot at t = 800 **τ**, when polymers starts to form small clusters, (c) A single cluster of three polymer molecules captured among many clusters formed at t = 800 **τ**, (d) Snapshot of the system at t = 50,000 **τ**. (e) Magnified image of a single micelle in the system, (f) An individual polymer molecule in a micelle bends into V-shape structure.

Author Manuscript Author Manuscript Author Manuscript Author Manuscript

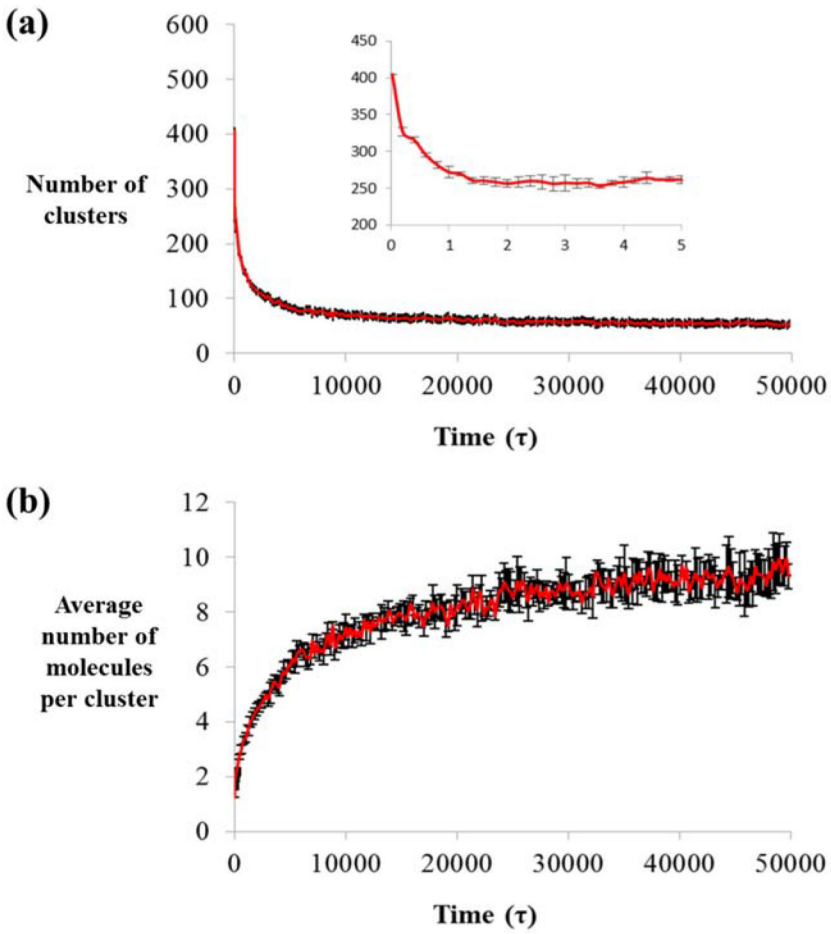

Figure 7:

Time evolution of (a) the number of clusters and (b) the average cluster size (that is, number of molecules) for a system with 504 Pluronic® F127 copolymers, as shown in Fig. 6. The inset in panel (a) shows the numbers of clusters from time 0 to 5τ.

Author Manuscript Author Manuscript Author Manuscript Author Manuscript

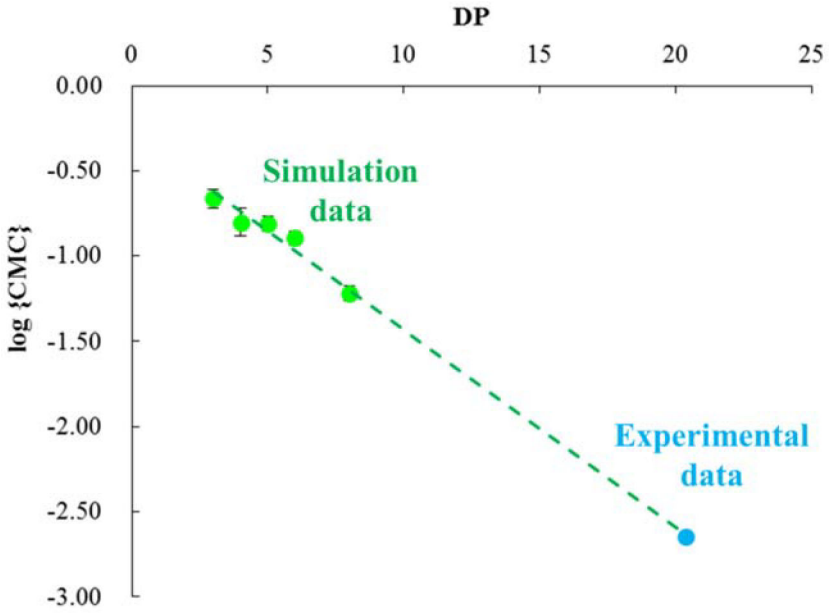

Figure 8:
Comparison of the simulated and experimentally determined CAC values of tyrospheres made of polymers with various DP of hydrophobic segment.

Author Manuscript

Author Manuscript

Author Manuscript

Author Manuscript

Table 1:

The soft repulsive interaction parameters for the coarse-grained PEG_{5k}-b-oligo(DTO-SA)-b-PEG_{5k} and Pluronic®.

a_{ij} **Tyrosene based polymer**	**Hydrophilic bead**	**Hydrophobic hard bead**	**Hydrophobic soft bead**	**Solvent**
Hydrophilic bead	25	100	100	25
Hydrophobic hard bead	100	25	55	100
Hydrophobic soft bead	100	55	25	100
Solvent	25	100	100	25

a_{ij} **Pluronics**	**Hydrophilic Bead**	**Hydrophobic bead**	**Solvent**
Hydrophilic Bead	25	100	25
Hydrophobic bead	100	25	100
Solvent	25	100	25

Author Manuscript

Author Manuscript

Author Manuscript

Author Manuscript

Table 2:

Dimension measurements for micelles encompassing tyrosine-based ABA copolymers with DP of 4, 8 and 18.

DP	Corona thickness (nm)	Core diameter (nm)	Micelle diameter (nm)
4	8.1 ± 0.7	7.9 ± 0.4	24 ± 2
8	8.1 ± 0.7	9.1 ± 0.9	25 ± 3
18	8.8 ± 2.2	15.4 ± 1.5	33 ± 6

Author Manuscript

Author Manuscript

Author Manuscript

Author Manuscript

Table 3:

The comparison of CAC values of Pluronic® copolymers F68, F88, F108, and F127 obtained from simulation and from experiments (pyrene method). The simulations have been run for a time interval of 20,000τ and each data point has been averaged over results from four independent simulations.

Pluronic	EO unit (x)	PO Unit (y)	Assignment of EO and PO beads for simulation (EO-PO-EO)	CAC(g/L)		
				Simulation (at 37 °C)	Experiment (at 37 °C)	Literature
F68	76.4	29.0	12 – 6 – 12	0.3 ± 0.1	0.44	1 at 20 °C[31]
F88	103.6	39.3	16 – 8 – 16	0.4 ± 0.1	1.29	6 at 40 °C[31]
F108	132.7	50.3	22 – 11 – 22	0.25 ± 0.04	0.33	0.4 at 40 °C[31]
F127	100.3	65.1	15 – 13 – 15	0.04 ± 0.01	0.05	0.08 at 40 °C[31]